JOURNAL OF SYNCHROTRON RADIATION
ISSN 1600-5775

Deep X-ray lithography system with a uniform and high-accuracy fabrication area established in beamline BL11 at NewSUBARU

Masaya Takeuchi,* Akinobu Yamaguchi and Yuichi Utsumi

Laboratory of Advanced Science and Technology for Industry, University of Hyogo, 3-1-2 Koto, Kamigori-cho, Ako-gun, Hyogo 678-1205, Japan. *Correspondence e-mail: masaya@lasti.u-hyogo.ac.jp

Received 15 August 2018
Accepted 19 December 2018

Edited by Y. Amemiya, University of Tokyo, Japan

Keywords: deep X-ray lithography; microfabrication; LIGA process.

A new lithography system to fabricate high-aspect-ratio 3D microstructures was developed at the NewSUBARU synchrotron radiation facility (University of Hyogo, Japan). The X-ray beam generated by this system has high parallelism (horizontal and vertical divergence angles of 278 µrad and 14 µrad, respectively) and high photon flux (31 mW mm^{-2} at a beam current of 300 mA). The high photon flux and exposure area of the system were validated and a beam-scan method for a large exposure area with a uniform dose distribution has been proposed. In addition, the deep X-ray lithography performance was characterized using a conventional photosensitive material and the synchrotron-radiation-induced direct etching of polytetrafluoroethylene (PTFE) was demonstrated. An enlargement of the microfabrication area up to 100 mm × 100 mm while contemporarily ensuring high uniformity was achieved.

1. Introduction

There have been rapid advances in the application of micro-devices as key functional components of hardware systems for several leading industries, such as automotive, electronics, information systems, energy and environment, fine chemistry, medicine, and biochemistry (Meng & Sheybani, 2014; Rebello, 2004; Vasiliev *et al.*, 2016; Elman & Upadhyay, 2010; Eddy & Sparks, 1998). Realizing high-precision steric microstructures integrating electrical, optical, mechanical and chemical functions in a restricted space could provide many advantages for such micro-devices. Hence, the importance of microfabrication techniques has further increased since they produce microstructures with a higher precision and aspect ratio, resulting in larger specific surface areas, which make the surface-related functions that the micro-devices are based on (*e.g.* electrostatic fields, surface tension and surface chemical reactions) intrinsically more significant. Deep X-ray lithography (DXL) using synchrotron radiation (Pantenburg *et al.*, 1998), a core process of lithographite, galvanofomung, abformung (LIGA) technology (Becker *et al.*, 1986), has great potential for fabricating specific devices for science and industrial fields requiring extreme resolution and a very high aspect ratio. It is not used for semiconductor applications, but its potential for large-volume mass-manufacturing can be greatly enhanced by improving the elementary processes and equipment with high stability, reliability and throughput. One of the advantageous properties of DXL over the other lithography techniques is the possibility of tuning its high penetration depth to specific resist (photosensitive polymer) heights by varying the photon energy of the X-rays emitted

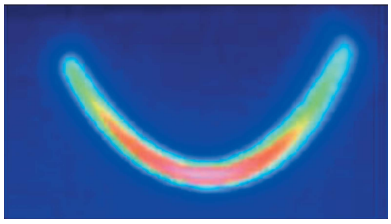

from the light source. From this perspective, the X-ray beamline plays a key role in controlling the X-ray properties and heightening the throughput of the lithography process.

In 2005, we designed and built a beamline for DXL (BL2) at the NewSUBARU synchrotron radiation facility (University of Hyogo, Japan) (Utsumi & Kishimoto, 2005; Utsumi *et al.*, 2005). Its X-ray lithography system can operate with two different energy regions, a high-energy region (2–12 keV) and a low-energy region (1–2 keV), selected according to the operation mode, X-ray lithography or DXL. The system can also perform large-area patterning across an A4-size area. The accuracy of the fabricated patterns could be improved by enhancing the parallelism of the X-ray beam emitted from the light source into the X-ray lithography chamber so that the penumbral blur would be reduced.

In this paper, we present the new BL11 DXL beamline that operates in the medium range (2–7 keV) of the spectrum used by BL2 and enhances the parallelism of the X-ray beam, providing horizontal and vertical divergence angles of 278 µrad and 14 µrad, respectively. Furthermore, the beamline enables a large processing area and a high photon flux of 31 mW mm^{-2} at a beam current of 300 mA. The DXL processing characteristics of BL11 were investigated and a newly developed beam-scan method was used to achieve a uniform X-ray intensity distribution on a work area up to 100 mm × 100 mm.

2. A beamline for deep X-ray lithography

Fig. 1 shows a side view (*a*) and a schematic (*b*) of the BL11 lithography system, which consists of X-ray optics and an exposure apparatus for DXL with a six-axis motion stage. The synchrotron radiation beam propagates with an enlarging cross section from the source point to a toroidal mirror (Pt coating on a single Si crystal) that collimates it into horizontal and vertical divergence angles of 278 µrad and 14 µrad, respectively. The incident angle to the toroidal mirror is optimized to cut the photon energy above 7 keV in accordance with the fabrication depth of DXL up to 1000 µm, while the photon energy below 2 keV is cut by two Be filters, with thicknesses of 300 µm and 125 µm, placed before the exposure apparatus for DXL.

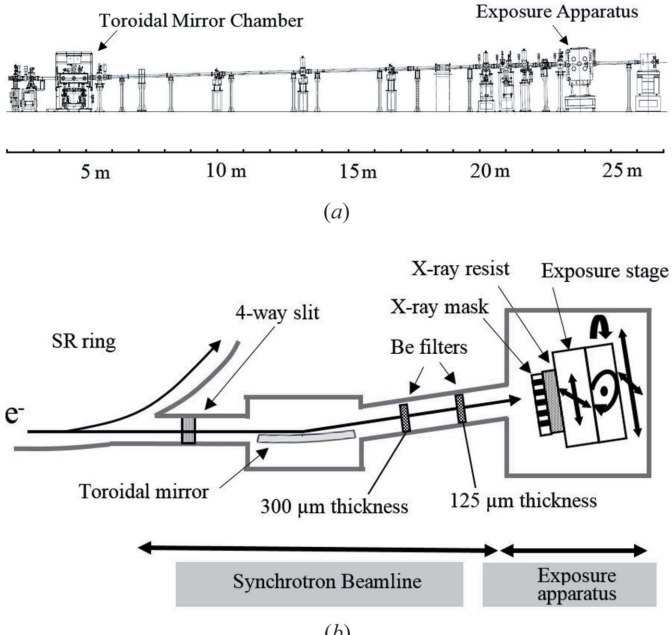

Figure 1
New BL11 deep X-ray lithography beamline at the NewSUBARU facility. (*a*) Detailed side view. (*b*) Schematic top view.

The spectrum of the X-ray beam generated by this system was calculated using *SPECTRA* (Tanaka & Kitamura, 2001). Fig. 2(*a*) shows the spectra of the beam at the exposure stage calculated for incidence angles of 0.6°, 0.7° and 0.8°. An incidence angle of 0.7° was more suitable given the DXL requirement of a medium spectrum band and the limitation due to the size of the toroidal mirror.

Fig. 2(*b*) shows the spectra of the beam at the exposure stage for storage ring energies of 1.0 GeV and 1.5 GeV, with a

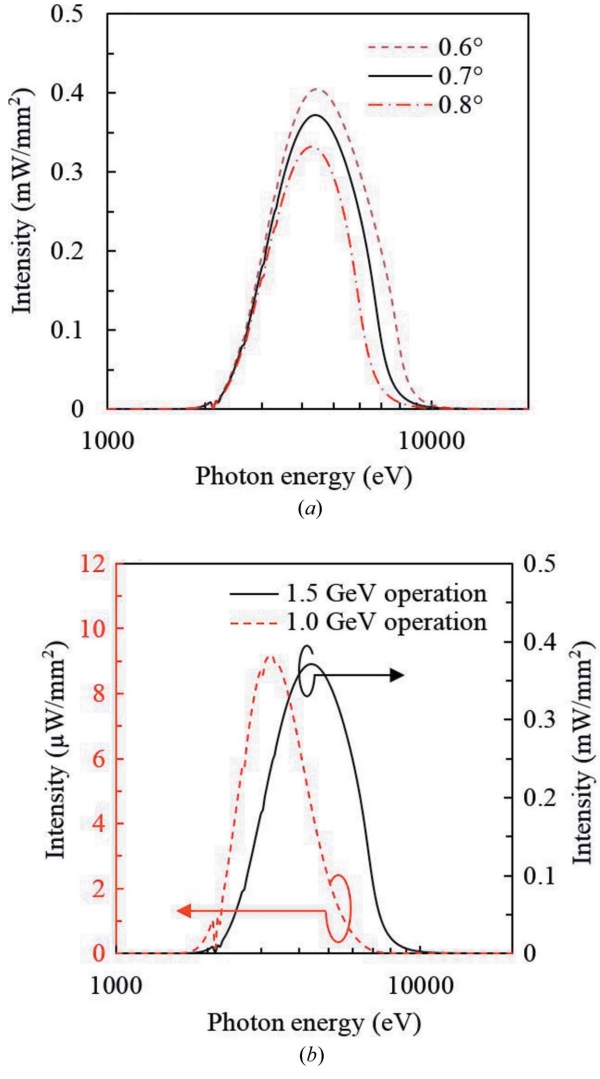

Figure 2
Calculated X-ray beam spectrum at the exposure stage of BL11 for (*a*) different incident angles to the toroidal mirror with 1.5 GeV operation and (*b*) different operation energies with a storage current of 300 mA.

storage ring current of 300 mA. The synchrotron radiation spectrum is selected by the absorber thickness of the X-ray mask, which also defines the lower limit of the line width of the desired lithography patterns since its aspect ratio is limited to less than two or three by the capability of UV and electron beam lithography technologies. The X-ray absorption increases with a decrease in the photon energy. Thus, to fabricate finer patterns (less than tens of micrometres), high-energy photons should be cut. A 1.0 GeV operation allows fabrication of a finer pattern because the high photon energy is significantly reduced, while the 1.5 GeV operation enables a high-throughput fabrication with a high-aspect-ratio microstructure because the photon flux in the higher energy range is two orders of magnitude higher than that with the 1.0 GeV operation.

Fig. 3 shows the intensity distribution (*a*) before and (*b*) after the toroidal mirror and (*c*) at the DXL exposure stage, as calculated by the ray-tracing program *SHADOW* (Lai & Cerrina, 1986). The horizontal and vertical acceptance angles of the synchrotron radiation beam emitted from the light source are 17.8 mrad and 2.2 mrad, respectively, and over 96% of the total photon flux could be in a vertical divergence angle range of ±0.32 mrad. The X-ray beam is collimated by the toroidal mirror and the simulation confirmed the resulting high parallelism with horizontal and vertical divergence angles of 278 µrad and 14 µrad, respectively, as well as the arc shaping of the cross-sectional intensity distribution, as shown in Fig. 3(*c*). In actual operations, part of both edges of the beam is cut in accordance with the opening diameters of the Be filters and the beam is directed to the exposure chamber. Figs. 3(*d*) and 3(*e*) show the integrated photon intensity distributions in the vertical and horizontal directions, respectively; the vertical photon number has an intense deviation compared with the horizontal one due to the beam shape.

3. Averaging the dose intensity by a two-dimensional scanning of the DXL operating stage

Fabricating a 3D microstructure with a representative length that is less than hundreds of micrometres is important since a 3D structure greatly improves the performance and functions of micro-devices and expands the applicable industrial field. Tabata *et al.* have fabricated a variety of 3D microstructures by using a moving X-ray mask (Tabata *et al.*, 2000), and Utsumi *et al.* obtained 3D microstructures for the optical waveguide panel of liquid crystal displays by controlling the 2D thickness distribution of the X-ray absorber (Utsumi *et al.*, 2004).

In our lithography system, such 3D fabrications can be achieved by adjusting the relative position between the X-ray mask and the resist-covered working substrate, the tilt and rotation angles, and the vertical and horizontal positions of the substrate as well as by simultaneous scanning during the exposure using the six-axis motion stage, as shown in Fig. 1(*b*). The exposure chamber can provide a helium atmosphere to reduce the thermal stress during the exposure of the substrate. The 2D temperature distribution in the substrate can be monitored using an infrared charge-coupled device camera. The exposure apparatus is also equipped with an anti-vibration mechanism for multi-axis motion stages.

The excessive heat load not only dissolves the resist but also degrades its photosensitive characteristics. Thus, it is important to suppress the thermal stress in the substrate within the proper temperature range. We measured the thermal and the heat load induced by synchrotron radiation irradiation on a sample substrate by using 3000 µm-thick polymethyl methacrylate (PMMA) sheets. Two operational states of the electron energy of the storage ring were tested, corresponding to 1.0 GeV and 1.5 GeV. For the 1.0 GeV operation and a storage ring current of 300 mA, without substrate scanning, the

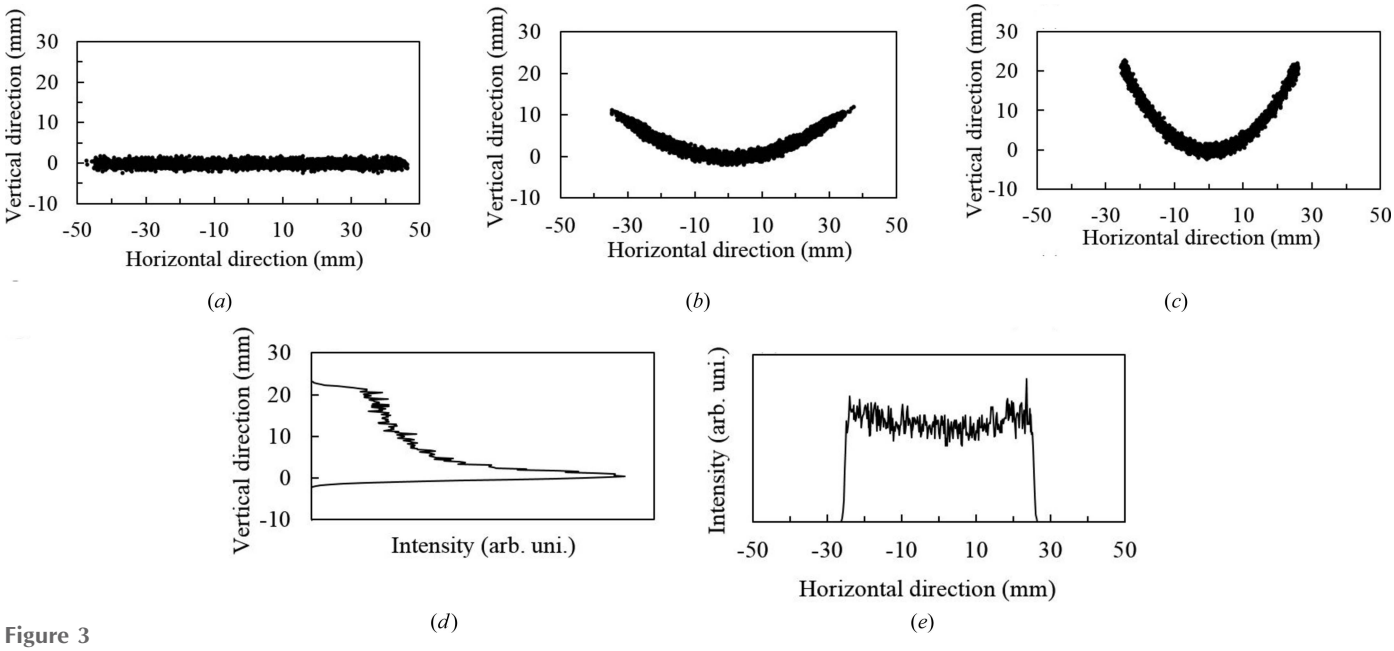

Figure 3
Calculated intensity distribution (*a*) before and (*b*) after the toroidal mirror and (*c*) at the deep X-ray lithography exposure stage; integrated photon numbers along the (*d*) vertical and (*e*) horizontal directions.

maximum temperature under both 10 Pa and 10 kPa He atmospheres was 40°C. For a 1.5 GeV operation and a storage ring current of 260 mA, without substrate scanning, the maximum substrate temperature under 10 kPa and 40 kPa He atmospheres was reduced to 160°C [Fig. 4(*a*)] and 155°C [Fig. 4(*b*)], respectively, compared with 190°C [Fig. 4(c)] under a vacuum. The difference in the maximum substrate temperature between the vacuum and the 10 kPa He atmosphere was remarkable, while it was lower than 5°C between the 10 kPa and the 40 kPa He atmospheres. Figs. 4(*d*) and 4(*e*) show the substrate temperature distribution under 10 kPa and 40 kPa He atmospheres with a vertical substrate scanning of 5 mm s^{-1}, which resulted in a reduction of the substrate temperature down to 60° and 55°, respectively. We confirmed that the exposure with substrate scanning can decrease the heat load on the PMMA enough to avoid the resist degradation induced by thermal stress.

We developed a scanning method that exposes a large-area sample to a uniform intensity distribution. As mentioned above, the intensity distribution of the X-ray beam has a non-uniform arc shape at the exposure position [Fig. 3(*c*)]. Thus, the integrated value of the photon number in the horizontal and vertical directions is also non-uniformly distributed, meaning that the integrated synchrotron radiation dose distribution is non-uniform when the beam only scans the sample linearly, in the horizontal or vertical direction. To solve this problem, we propose a 2D scanning method that combines the scanning directions along the *x* and the *y* axes, as shown in Fig. 5(*a*). First, the X-ray beam is scanned on the resist surface in the *y* direction outside the patterning area and shifted in the *x* direction by one pitch. Then it moves back in the *y* direction. By repeating these operations, the entire patterning area of the sample is irradiated, with the condition that the substrate scanning in the *x* direction is executed outside the patterning area. Fig. 5(*b*) shows the calculated exposure intensity distribution with a pitch of 1 mm in the *x* direction at $y = 0$. A periodic intensity variation, derived from the width of the pitch, can be observed due to the beam-scan method. The maximum deviation subtending the average intensity from −50 mm to 50 mm along the *x* direction was below 3%.

Based on this calculation result, we exposed a sample using the method illustrated in Fig. 5(*a*) with a pitch of 1 mm to investigate its processing characteristics. PMMA sheets (100 mm × 100 mm) of thickness 1500 µm were used as the photosensitive material. The GG developer (60% diethylene glycol, 20% morpholine, 15% pure water, 5% ethanolamine) was also used and the development condition was submergence for 24 h at 25°C. The processing depth was measured with a laser microscope (Keyence Co. Ltd, VK-8510). Fig. 5(*c*) shows the measurement points; each point was 1 mm wide in the *x* direction and measured with a resolution depth of 10 nm. Figs. 5(*d*) and 5(*e*) show the measurement results; the maximum deviation subtending the average processing depth was below 3% with a 1.5 GeV operation and below 4% with 1.0 GeV. These values correspond to the above-calculated value. By this method, we could obtain a uniform X-ray intensity distribution on a sample substrate in a 100 mm × 100 mm area.

4. Demonstration of DXL patterning and synchrotron-radiation-induced photochemical etching of PTFE

As mentioned above, the X-ray spectrum in our system in the 2–7 keV range is obtained with a 1.5 GeV operation, while the 1.0 GeV operation reduces the photon energy below 5 keV [Fig. 2(*b*)]. The operation mode is selected depending on the required line width, shape, processing depth, accuracy and throughput. Hence, evaluating the influence of the exposure/development characteristics from the difference in the spectra of the two operation modes is essential.

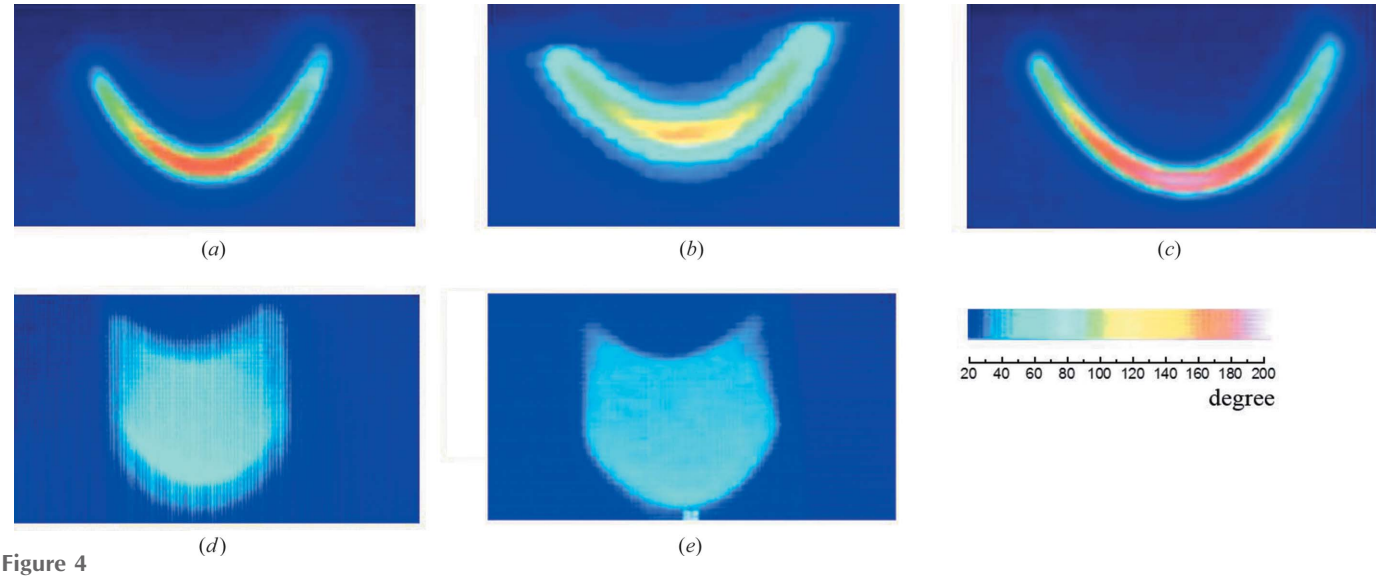

Figure 4
Temperature distribution in a 3000 µm-thick PMMA sheet during X-ray exposure with the 1.5 GeV operation. (*a*) Under 10 kPa He atmosphere vacuum without scanning; (*b*) under 40 kPa He atmosphere vacuum without scanning; (*c*) in vacuum without scanning; (*d*) under 10 kPa He atmosphere with 5 mm s^{-1} scanning; (*e*) under 40 kPa He atmosphere with 5 mm s^{-1} scanning.

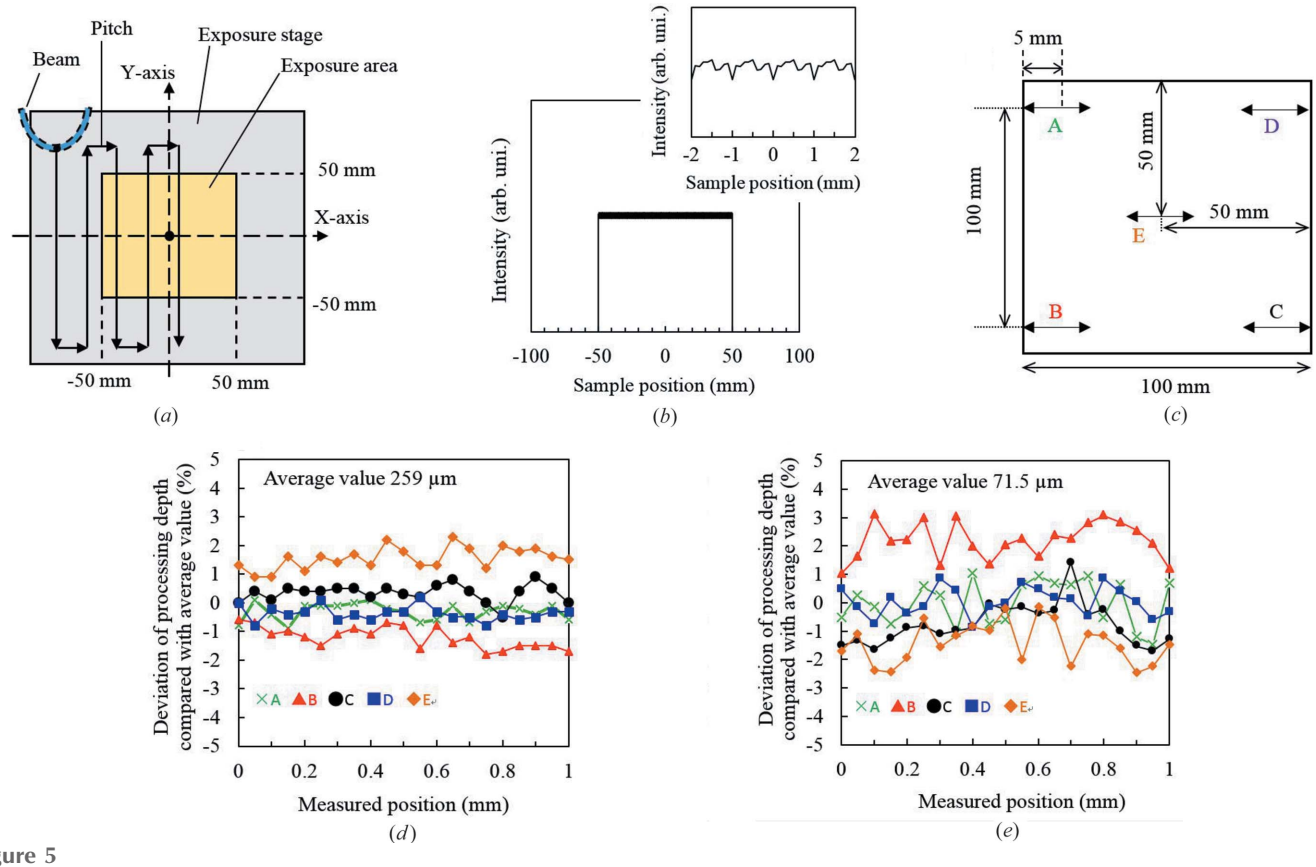

Figure 5
(*a*) Beam-scan method. (*b*) Calculated intensity distribution at $y = 0$. (*c*) Laser measurement points for the processing depth of the sample. (*d*) and (*e*) Measurement results for 1.5 GeV and 1.0 GeV operations.

We investigated the DXL performance of our system and its capability of synchrotron-radiation-induced photochemical etching by using PTFE. The exposure-dose dependence of the processing depth was also analysed. A 1500 µm-thick PMMA sheet was used as the resist for X-ray exposure. The sheet with a 1000 µm-thick stainless steel (SUS) stencil mask was placed on the multi-axis exposure stage and scanned using the above-mentioned 2D method, as shown in Fig. 6(*a*), with a scanning width of 20 mm and a speed of 5 mm s^{-1}. The exposure dose to the resist was controlled by changing the number of scans, and its relationship with the processing depth of the PMMA sheet is shown in Fig. 6(*b*). A processing depth of about 900 µm was obtained with a 1.5 GeV operation, which clearly proves the significant effects that are a result of the operation mode. This result is attributed to the difference in the two spectral bands shown in Fig. 2(*b*), meaning that the difference in the penetration depth of the X-ray dose depends on the photon energy.

Furthermore, we achieved a DXL patterning with high uniformity on a large working area. We used a SUS stencil mask and a membrane mask [Fig. 7(*a*)] fabricated by electroforming and wet etching. The absorber of the SUS mask was 100 µm thick. The membrane mask consisted of a 7.5 µm-thick Au layer as the absorber and a 15 µm-thick polyimide film as the membrane. Fig. 7(*b*) shows the result of large-area patterning of the PMMA sheet by our beam-scan method, as shown in Fig. 5(*a*), with a pitch of 1 mm and a 1.5 GeV

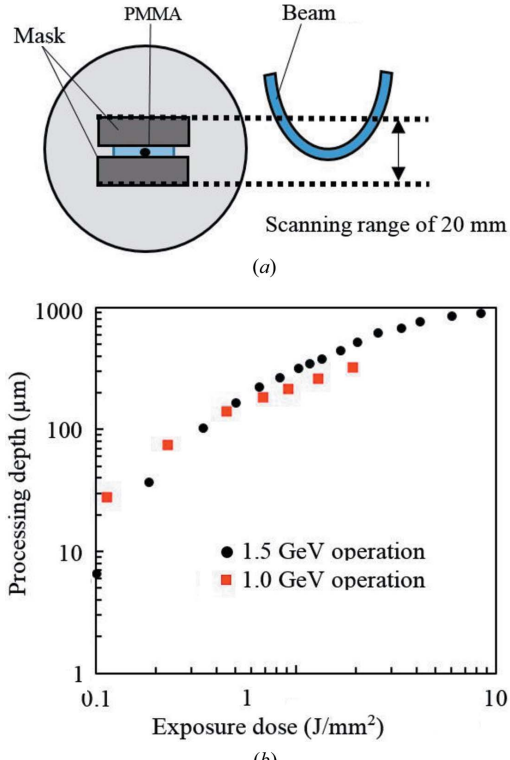

Figure 6
(*a*) Scanning of a PMMA sheet mounted on the multi-axis exposure stage. (*b*) Exposure-dose dependence of the processing depth of the PMMA sheet for 1.5 GeV and 1.0 GeV operations.

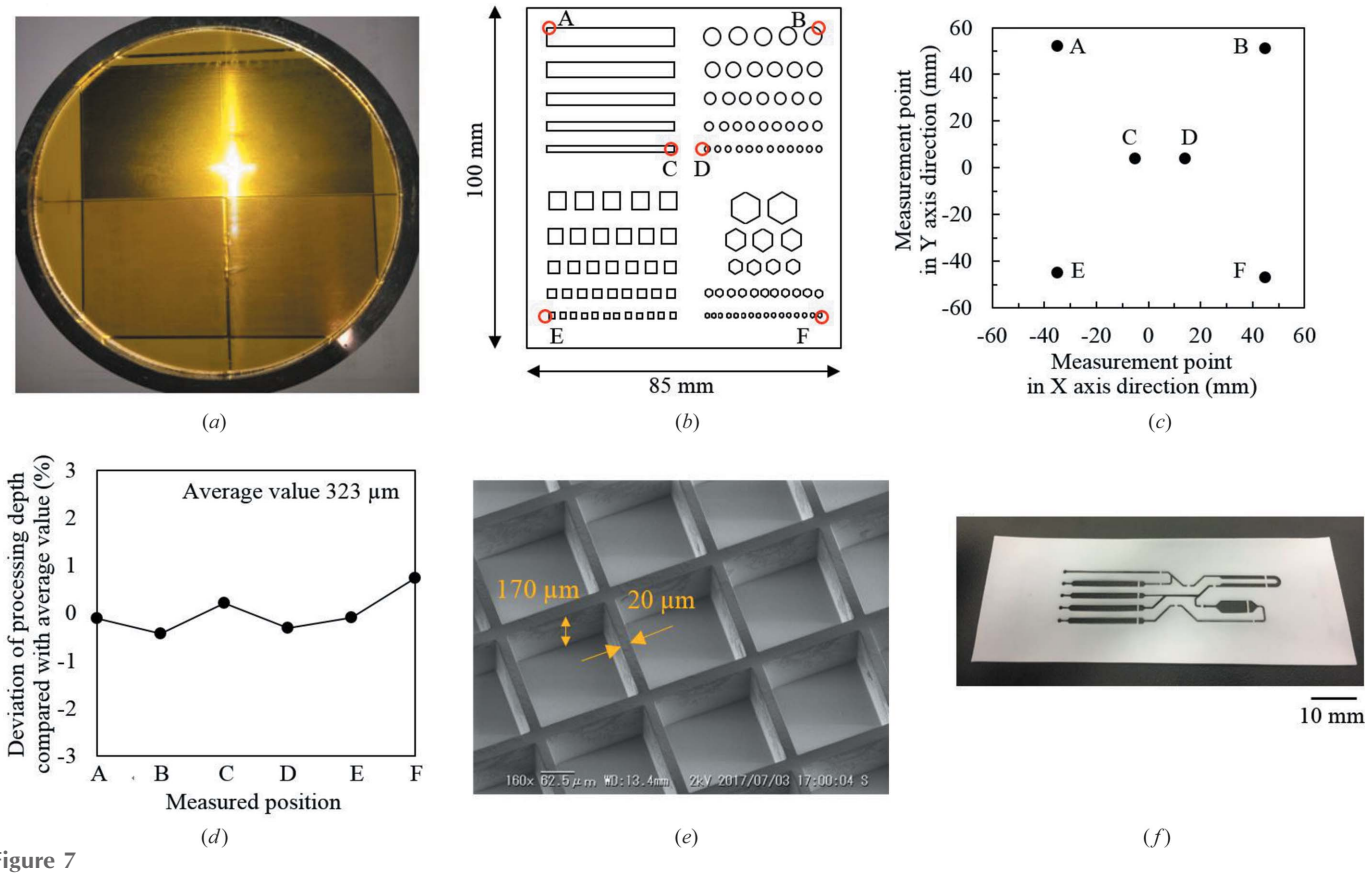

Figure 7
(*a*) Membrane mask. (*b*) Large-area patterning of the PMMA sheet by the proposed beam-scan method. (*c*) Coordinate of the measurement points. (*d*) Deviation of the measurement results for a 1.5 GeV operation. (*e*) Pattern fabricated with the 1.0 GeV operation. (*f*) PTFE dry etched with a 1.5 GeV operation.

operation. The average processing depth from point A to point F, shown in Fig. 7(*c*), was 323 µm and the deviations were below 1% [Fig. 7(*d*)]. This demonstrates our success in obtaining a uniform processing depth on a large patterning area of 85 mm × 100 mm. Fig. 7(*e*) shows the result of DXL pattering using the polyimide membrane mask shown in Fig. 7(*a*) with a 1.0 GeV operation.

The synchrotron-radiation-induced photochemical direct etching of PTFE (Ukita *et al.*, 2008; Yamaguchi *et al.*, 2016; Inayoshi *et al.*, 1995; Zhang *et al.*, 1995) was also demonstrated using the DXL system. PTFE is expected to generate many functional advantages for micro-devices, such as high-frequency circuits, microreactors and micro total analysis systems (µTAS) for bioscience and medical use, since it has excellent characteristics such as high heat and chemical resistance, low friction coefficient, high insulation, and low electric permittivity compared with other polymeric materials. However, the microfabrication of PTFE is made difficult by such characteristics, but we have achieved its synchrotron-radiation-induced direct etching by using soft X-rays at the NewSUBARU facility. In this study, the microfabrication of PTFE was also carried out with a 1.5 GeV operation by using our DXL system. The PTFE substrate temperature was 200°C and the total exposure dose was 11 J mm^{-2}, with a beam-scan speed of 1 mm s^{-1}. Fig. 7(*f*) shows an obtained µTAS device for derivatization of amino acids obtained by direct etching of PTFE with a comparatively high precision, achieved using the new DXL system of BL11.

5. Conclusions

We established and evaluated the performance of the new BL11 X-ray lithography beamline at the NewSUBARU facility, which provides a high photon flux and a high parallelism of the X-ray beam, with horizontal and vertical divergence angles of 278 µrad and 14 µrad, respectively, enabling large processing areas. We also developed a beam-scan method for averaging the dose intensity distribution, achieving a uniform depth distribution on a 100 mm × 100 mm PMMA sheet with a maximum deviation of <4%. We successfully performed DXL microfabrication on an 85 mm × 100 mm PMMA sheet with a maximum depth deviation of 1%. Furthermore, we obtained a µTAS device for the derivatization of amino acids with comparatively high precision by direct etching of PTFE with a 1.5 GeV operation. Our new DXL system can allow high accurate steric microfabrication with a high aspect ratio and uniform processing depth.

References

Becker, E., Ehrfeld, W., Hagmann, P., Maner, A. & Münchmeyer, D. (1986). *Microelectron. Eng.* **4**, 35–56.

Eddy, D. & Sparks, D. (1998). *Proc. IEEE*, **86**, 1747–1755.
Elman, N. & Upadhyay, U. (2010). *Curr. Pharm. Biotechnol.* **11**, 398–403.
Inayoshi, M., Ikeda, M., Hori, M., Goto, T., Hiramatsu, M. & Hiraya, A. (1995). *Jpn. J. Appl. Phys.* **34**, L1675–L1677.
Lai, B. & Cerrina, F. (1986). *Nucl. Instrum. Methods Phys. Res. A*, **246**, 337–341.
Meng, E. & Sheybani, R. (2014). *Lab Chip*, **14**, 3233–3240.
Pantenbrug, F., Achenbach, S. & Mohr, J. (1998). *Microsystem Tech.* **4**, 89–93.
Rebello, K. (2004). *Proc. IEEE*, **92**, 43–55.
Tabata, O., Terasoma, K., Agawa, N. & Yamamoto, K. (2000). *IEEJ Trans. Sensors Micromachines*, **120**, 321–326.
Tanaka, T. & Kitamura, H. (2001). *J. Synchrotron Rad.* **8**, 1221–1228.
Ukita, Y., Kishihara, M., Kanda, K., Matsui, S., Mochiji, K. & Utsumi, Y. (2008). *Jpn. J. Appl. Phys.* **47**, 337–341.
Utsumi, Y. & Kishimoto, T. (2005). *J. Vac. Sci. Technol. B*, **23**, 2903–2909.
Utsumi, Y., Kishimoto, T., Hattori, T. & Hara, H. (2005). *Jpn. J. Appl. Phys.* **44**, 5500–5504.
Utsumi, Y., Minamitani, M. & Hattori, T. (2004). *Jpn. J. Appl. Phys.* **43**, 3872–3876.
Vasiliev, A., Sokolov, A., Pisliakov, A., Oblov, K., Samotaev, N., Kim, V., Tkachev, S., Gubin, S., Potapov, G., Kokhtina, Yu. & Nisan, A. (2016). *IOP Conf. Ser. Mater. Sci. Eng.* **151**, 012024.
Yamaguchi, A., Kido, H., Ukita, Y., Kishihara, M. & Utsumi, Y. (2016). *Appl. Phys. Lett.* **108**, 051610.
Zhang, Y., Katoh, T., Washio, M., Yamada, H. & Hamada, S. (1995). *Appl. Phys. Lett.* **67**, 872–874.